Robust fiber-based frequency synchronization system immune to strong temperature fluctuation

Xi Zhu (朱 玺)[1,2], Bo Wang (王 波)[1,*], Yichen Guo (郭倚辰)[1], Yibo Yuan (袁一博)[2], Romeo Gamatham[3], Bruce Wallace[3], Keith Grainge[4], and Lijun Wang (王力军)[1,2]

[1]*State Key Laboratory of Precision Measurement Technology and Instruments, Department of Precision Instrument, Tsinghua University, Beijing 100084, China*

[2]*Department of Physics, Tsinghua University, Beijing 100084, China*

[3]*SKA South Africa, Blend on Baker, Rosebank 2196, Johannesburg, South Africa*

[4]*Jodrell Bank Centre for Astrophysics, Alan Turing Building, School of Physics & Astronomy, The University of Manchester, Oxford Road, Manchester M13 9PL, UK*

**Corresponding author: bo.wang@tsinghua.edu.cn*

Received September 8, 2017; accepted November 16, 2017; posted online December 5, 2017

In order to make the fiber-based frequency synchronization system suitable for the use of large-scale scientific and engineering projects in which the ambient temperature of the fiber links change dramatically, we design a non-harmonic frequency dissemination system immune to strong temperature fluctuation. After the lab tests, in which the ambient temperature of the fiber fluctuates 40°C/day and 20°C/h, respectively, the relative frequency stabilities of this system reaches 4.0×10^{-14}/s and $3.0 \times 10^{-16}/10^4$ s. It is demonstrated that the proposed non-harmonic scheme shows a strong robustness to complicated working environment with strong temperature fluctuation.

OCIS codes: 060.0060, 120.0120.
doi: 10.3788/COL201816.010605.

As the world's largest radio telescope under construction, the Square Kilometre Array (SKA) consists of thousands of parabolic dishes and aperture arrays, which work together to form a one-square-kilometer collecting area. SKA will surpass any current telescope and help us further understand the universe. To ensure sufficient imaging fidelity, all of the telescopes should keep time and be frequency synchronized with stabilities superior to 2.3×10^{-12}/s, 3.8×10^{-14}/min, and $1.9 \times 10^{-14}/10$ min[1]. In 2015, we proposed and demonstrated a precision reference frequency synchronization scheme via 1f–2f dissemination, according to the requirements and characteristics of SKA[2]. Here, we name it a harmonic system. It features the phase-noise compensation performed at the client site to reduce space requirement and unnecessary complexity at central station. Considering our previous work along with the existing fiber-based time and frequency transfer schemes demonstrated by different groups[3–17], they almost utilized fiber spools or urban telecommunication fibers, which basically run in buried cables. While for large-scale scientific and engineering facilities, such as SKA, on account of attractive infrastructure cost and simple laying, overhead fiber links will be adopted. Unfortunately, the overhead fiber links are affected by atmospheric temperature variation and mechanical stress. Consequently, they are much noisier than fiber spools and buried fiber[18–25]. Taking the SKA South Africa site for an example, it is constructed in the desert region. From the meteorological parameters captured by the local weather station, rapid temperature change caused by a thunderstorm, gale, sunrise, and sunset is recorded frequently in the past. According to statistical analysis on the temperature data in the period from January 1, 2005 to March 31, 2011, the daily temperature fluctuation can reach 40°C[26]. Therefore, a robust frequency dissemination system immune to strong temperature fluctuation is required.

After the performance test in the lab, the harmonic system was shipped to the SKA South Africa site to perform an outfield test on several overhead fiber links from the 19th to 27th September 2015. The frequency dissemination stability with phase-noise compensation via the 64 km overhead fiber is shown in Fig. 1. For easy comparison, the dissemination stability of 32 km overhead fiber without compensation is also shown in Fig. 1. During the field test, we did not measure the dissemination stability on 64 km overhead fiber without compensation, but it will be worse than that on 32 km overhead fiber[27]. It can be seen that there is a bump on the Allan deviation plot of dissemination stability at the averaging time between 10 and 100 s, which had not shown up in previous lab tests using fiber spools. Through theoretical analysis and experimental verification, as described later, we find that the fiber-induced phase fluctuation due to strong temperature change cannot be completely compensated.

In this Letter, we analyze the reason why the previous harmonic scheme is not perfectly immune to temperature fluctuation and attribute this imperfection to limited isolation and nonlinear performance of the radio frequency (RF) components in the system. According to the analysis, we design a non-harmonic system and test its performance in an environment with temperature fluctuating 40°C per day, which is similar to the temperature

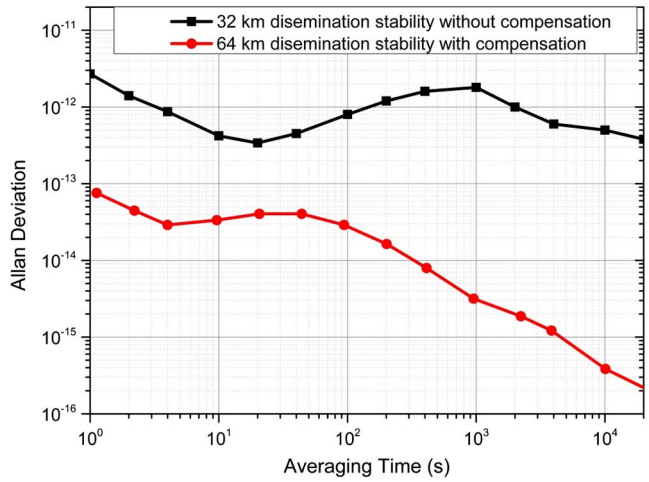

Fig. 1. (Color online) Frequency dissemination stability result with and without phase-noise compensation through overhead fiber at the SKA South African site.

fluctuation of the SKA South Africa site. The result of this test shows a frequency dissemination stability of $4.0 \times 10^{-14}/\mathrm{s}$ and $3.0 \times 10^{-16}/10^4$ s. Furthermore, we carry out another test under the situation of rapid temperature change—20°C per hour—and obtain a frequency dissemination stability of $3.0 \times 10^{-14}/\mathrm{s}$ and $3.0 \times 10^{-16}/10^4$ s. Based on these test results, we conclude that the nonharmonic frequency dissemination system is robust with both huge and rapid temperature fluctuation and, hence, is capable of operating in severe environments of large-scale scientific and engineering projects.

The schematic diagram of the harmonic reference frequency synchronization scheme is shown in Fig. 2. One transmitting site (TX) consists of several extensible disseminating channels, so that it has the ability to simultaneously collaborate with several receiving sites (RXs). Here, we just take one channel, for example, to explain the concept. At the TX, the 100 MHz frequency signal from an H-maser acts as the reference signal. A phase-locked dielectric resonant oscillator (PDRO) with a frequency of 2 GHz is phase-locked to it and can be expressed as

$$V_0 = \cos(\omega_0 t + \phi_0). \tag{1}$$

It is used to modulate the amplitude of a 1547.72 nm diode laser (Laser A). Then, the modulated laser light

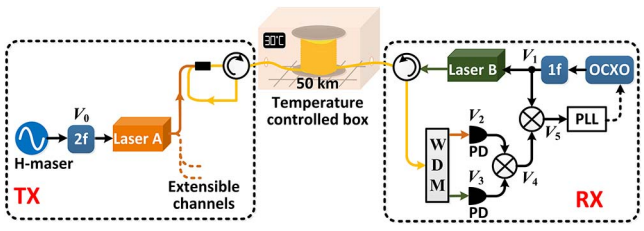

Fig. 2. Schematic diagram of the harmonic reference frequency synchronization scheme.

is divided into several equal light beams. After passing through a fiber coupler and an optical circulator, the light beam is disseminated from the TX to the corresponding RX via a fiber link. At the RX, another PDRO with a frequency of 1 GHz is phase-locked to a 100 MHz oven-controlled crystal oscillator (OCXO). The 1 GHz signal can be expressed as

$$V_1 = \cos(\omega_1 t + \phi_1), \tag{2}$$

and is used to modulate the amplitude of a 1548.53 nm diode laser (Laser B). After passing through an optical circulator, the modulated laser light is coupled into the same fiber link and disseminated via the route RX–TX–RX. At the RX, the disseminated laser lights are separated from each other by a wavelength-division multiplexer (WDM). Two photodiodes (PDs) are used to recover the disseminated frequency signals, which can be expressed as

$$V_2 = \cos(\omega_0 t + \phi_0 + \phi_p), \tag{3}$$

$$V_3 = \cos(\omega_1 t + \phi_1 + \phi_p'). \tag{4}$$

Here, ϕ_p represents the phase fluctuation induced by the 50 km fiber dissemination for the 2 GHz signal V_0, and ϕ_p' represents that of the 50 km fiber round-trip dissemination for the 1 GHz signal V_1. The one-way accumulated phase fluctuation of the 2 GHz frequency signal is the same as the round-trip phase fluctuation of the 1 GHz frequency signal, namely $\phi_p = \phi_p'$. By frequency mixing down V_2 and V_3, we can get a 1 GHz signal:

$$V_4 = \cos[(\omega_0 - \omega_1)t + \phi_0 + \phi_p - \phi_1 - \phi_p']. \tag{5}$$

Then, V_4 is frequency mixed with V_1, and the generated DC signal can be expressed as

$$V_5 = \cos[(\omega_0 - 2\omega_1)t + \phi_0 + \phi_p - 2\phi_1 - \phi_p']. \tag{6}$$

As an error signal, V_5 is used to feedback-control the phase of the OCXO by a phase-locked loop (PLL). With the relations of $\omega_0 = 2\omega_1$, and $\phi_p = \phi_p'$, V_5 can be expressed as

$$V_5 = \cos(\phi_0 - 2\phi_1). \tag{7}$$

When the PLL is closed, the OCXO at the RX is phase-locked to the reference signal at the TX, namely, $\phi_0 = 2\phi_1$. Thus, the reference signal is recovered at the RX.

Here, to simulate the ambient temperature fluctuation of the SKA South Africa site, the fiber spool is placed in a temperature-controlled box, and its temperature fluctuation is set to be 10°C, 20°C, 30°C, and 40°C per day, respectively, as Fig. 3(a) shows. The corresponding relative frequency stability between the 100 MHz reference signal and the recovered 100 MHz signal is shown in Fig. 3(b). We can see from the results that when the

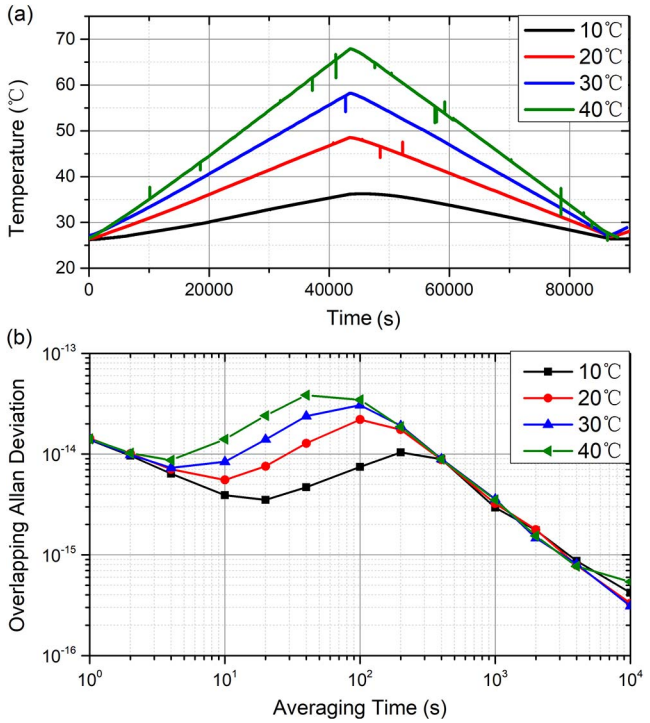

Fig. 3. (Color online) (a) Ambient temperature of the fiber link fluctuating 10°C, 20°C, 30°C, and 40°C per day. (b) Measured frequency dissemination stability with strong temperature fluctuation.

ambient temperature of the fiber link fluctuates, a bump shows up on the Allan deviation plot at the averaging time between 10 and 1000 s. The position of bump varies according to different temperature fluctuations.

Even though the measured stability can fulfill the SKA requirement, we still made an analysis on the bump and solved it. In the previous discussion, the frequency mixing between V_2 and V_3 is considered to be an ideal process. That is to say, the output signal V_4 just contains the ideal signal [see Eq. (5)]. Nevertheless, influenced by the limited isolation and nonlinear performance of the frequency mixer in the system, components of the output signal V_4 are complex. Owing to the desired output signal with the frequency of 1 GHz, the leakage of V_3 with the same frequency cannot be filtered. It would limit the frequency dissemination stability. The frequency mixer we used (Marki T3-03) features a high third-order intercept point (IP3) that it can reduce the unwanted nonlinear effect, but the influence still exists. The frequency signals V_2 and V_3 in Taylor's series can be expressed as

$$V_2 = \cos(\omega_0 t + \phi_0 + \phi_p) + a_1 \cos(2\omega_0 t + 2\phi_0 + 2\phi_p) + a_2 \cos(3\omega_0 t + 3\phi_0 + 3\phi_p) + \cdots, \quad (8)$$

$$V_3 = \cos(\omega_1 t + \phi_1 + \phi'_p) + b_1 \cos(2\omega_1 t + 2\phi_1 + 2\phi'_p) + b_2 \cos(3\omega_1 t + 3\phi_1 + 3\phi'_p) + \cdots, \quad (9)$$

where a and b are coefficients. The components of these two signals are frequency mixed with each other. Through a 1 GHz band pass filter, the output signal V_4 can be expressed as

$$V_4 = \cos[(\omega_0 - \omega_1)t + \phi_0 + \phi_p - \phi_1 - \phi'_p] + \xi \cos(\omega_1 t + \phi_1 + \phi'_p) + \zeta \cos[(3\omega_1 - \omega_0)t + 3\phi_1 + 3\phi'_p - \phi_0 - \phi_p] + \cdots, \quad (10)$$

where ξ and ζ are small coefficients. The first term is the ideal signal, the second is the leakage of V_3, and the third is produced by the third harmonic of V_3 frequency mixing with V_2. Since other higher order harmonics and products are much smaller, we just take these two influence factors into consideration. Considering $\phi_p = \phi'_p$, V_5 can be expressed as

$$V_5 = \cos(\phi_0 - 2\phi_1) + \xi \cos(\phi_p) + \zeta \cos(2\phi_1 + 2\phi_p - \phi_0). \quad (11)$$

The continuous variation of ϕ_p will lead to periodic variation of the second and third terms of V_5 in Eq. (11). Thus, the phase ϕ_1, which is tunable by changing the control voltage of the OCXO, will also vary periodically when the PLL is closed, instead of being completely equal to $\frac{1}{2}\phi_0$ as expected. Consequently, the Allan deviation plot of the frequency dissemination stability in Fig. 3(b) has a bump on it. Indeed, in our experiment, we find the power of the third-harmonic component is one-hundred times smaller than that of the 1 GHz leakage component. Here, we will mainly consider the 1 GHz leakage in the analysis. The phase item ϕ_1 will be disturbed at the same period with $\cos(\phi_p)$.

Considering the mechanical tension coefficients of fiber length and refractive index, the effective temperature coefficient of phase time delay is 76 $\frac{\text{ps}}{\text{km}\cdot\text{°C}}$[28]. For the signal frequency of 2 GHz and the fiber length of 50 km, the temperature coefficient of phase delay should be

$$\frac{\mathrm{d}\phi_p}{\mathrm{d}T} = 15.2\pi \text{ rad/°C}. \quad (12)$$

Taking the temperature fluctuating 40°C/day as an example, the temperature changing rate is $\frac{\mathrm{d}T}{\mathrm{d}t} = \frac{1}{1080}$ °C/s (increasing or decreasing 40°C in 12 h). According to Eq. (12), the phase delay changing rate can be calculated as

$$\frac{\mathrm{d}\phi_p}{\mathrm{d}t} = \frac{\mathrm{d}\phi_p}{\mathrm{d}T} \cdot \frac{\mathrm{d}T}{\mathrm{d}t} = 15.2\pi \cdot \frac{1}{1080} = 0.014\pi \text{ rad/s}. \quad (13)$$

Correspondingly, the period of $\cos(\phi_p)$ is $\frac{2\pi}{0.014\pi} = 140$ s, which is the same with the disturbance period of ϕ_1.

Consequently, the horizontal position of the bump on the Allan deviation plot should be at half of the period, which is 70 s. As to the temperature fluctuating 10°C, 20°C, and 30°C per day, the horizontal positions should be 280, 140, and 93 s, respectively. These calculated results agree with the test results shown in Fig. 3(b).

The schematic diagram of the non-harmonic precision reference frequency synchronization scheme is shown in Fig. 4.

The TX remains the same. Namely, the expression of V_0 is the same as Eq. (1). After fiber dissemination from the TX to the RX, the expression of V_2 is also the same as in Eq. (3). At the RX, the 1 GHz signal from the PDRO of the previous scheme is replaced by two signals, $1f_a$ and $1f_b$, from frequency synthesizers with a frequency of 1 GHz + 130 Hz and 1 GHz − 130 Hz, respectively. Both of them are phase-locked to the same OCXO. Then, V_1 can be expressed as

$$V_1 = \cos[(\omega_1 + 130\,\mathrm{Hz})t + \phi_1], \tag{14}$$

and V_3 can be expressed as

$$V_3 = \cos[(\omega_1 + 130\,\mathrm{Hz})t + \phi_1 + \phi_p']. \tag{15}$$

By frequency mixing down V_2 and V_3, the down-conversion signal can be expressed as

$$\begin{aligned} V_4 = {} & \cos[(\omega_0 - \omega_1 - 130\,\mathrm{Hz})t + \phi_0 + \phi_p - \phi_1 - \phi_p'] \\ & + \xi\cos[(\omega_1 + 130\,\mathrm{Hz})t + \phi_1 + \phi_p'] \\ & + \zeta\cos[(3\omega_1 - \omega_0 + 390\,\mathrm{Hz})t + 3\phi_1 + 3\phi_p' - \phi_0 - \phi_p]. \end{aligned} \tag{16}$$

The second term is the leakage of V_3, and the last term is produced by the third harmonic of V_3 mixing with V_2. The frequency signal $1f_b$ is used for frequency mixing, and it can be expressed as

$$V_6 = \cos[(\omega_1 - 130\,\mathrm{Hz})t + \phi_6], \tag{17}$$

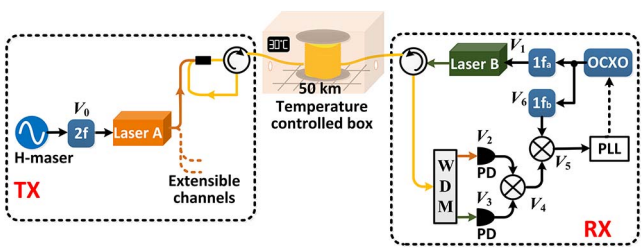

Fig. 4. Schematic diagram of non-harmonic precision reference frequency synchronization scheme. $1f_a$, 1 GHz + 130 Hz signal phase-locked to OCXO; $1f_b$, 1 GHz − 130 Hz signal phase-locked to OCXO.

where ϕ_6 can be considered the same as ϕ_1 with negligible difference. Then, V_6 is mixed with V_4. An error signal is obtained:

$$\begin{aligned} V_5 = {} & \cos(\phi_0 + \phi_p - 2\phi_1 - \phi_p') \\ & + \xi\cos(260\,\mathrm{Hz} \times t + \phi_p') \\ & + \zeta\cos(520\,\mathrm{Hz} \times t + 2\phi_1 + 3\phi_p' - \phi_0 - \phi_p). \end{aligned} \tag{18}$$

Through a low pass filter, the last two terms can be filtered. In this non-harmonic scheme, the relation of phase fluctuation compensation becomes $(1 + 1.3 \times 10^{-7})\phi_p = \phi_p'$. Then, V_5 can be expressed as

$$V_5 = \cos(\phi_0 - 2\phi_1 - 1.3 \times 10^{-7}\phi_p). \tag{19}$$

When the PLL is closed, it will be

$$\phi_0 = 2\phi_1 + 1.3 \times 10^{-7}\phi_p. \tag{20}$$

A little part of ϕ_p is brought into the error signal. Taking the temperature fluctuating 40°C as an example, the residual phase error $1.3 \times 10^{-7}\Delta\phi_p$ is 1.9×10^{-14} s, which can be neglected.

With the ambient temperature of the fiber link fluctuating 40°C/day, which is similar to the temperature fluctuation of the SKA South Africa site, we measure relative frequency stabilities between 100 MHz reference signal and recovered signal after 50 km dissemination. The result is shown in Fig. 5. The bump on the Allan deviation plot of dissemination stability at the averaging time between 10 s and 1000 s almost diminished, and relative frequency stabilities of 4.0×10^{-14}/s and $3.0 \times 10^{-16}/10^4$ s are obtained. For easy comparison, the dissemination stability of

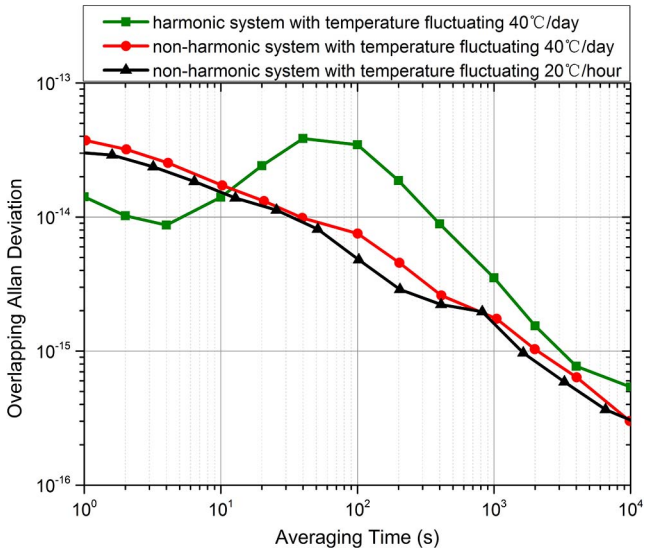

Fig. 5. (Color online) Measured frequency dissemination stabilities of non-harmonic system for 50 km distance with temperature fluctuating 40°C/day and 20°C/h.

the harmonic system with the temperature fluctuating 40°C/day is also shown in Fig. 5.

Furthermore, to test the performance of this non-harmonic system under rapid temperature fluctuation, we conduct another experiment, in which the ambient temperature of the fiber spool varies 20°C/h. There is also no bump on the Allan deviation plot, and the relative frequency stability reaches 3.0×10^{-14}/s and $3.0 \times 10^{-16}/10^4$ s, as shown in Fig. 5.

For the proposed scheme, a small part of the phase noise induced by the fiber link is left intentionally uncompensated. They are the reasons why the short term stability of the non-harmonic system is worse than the harmonic system, as shown in Fig. 5. However, for the non-harmonic system, the advantages are that it is not affected by the limited isolation and nonlinear performance of RF components in the system anymore. Also, it is more suitable for practical applications with strong temperature fluctuation.

In conclusion, we design a non-harmonic synchronization scheme and prove it to be immune to strong temperature fluctuations and, hence, is capable of operating in severe environments of large-scale scientific and engineering projects.

This work is being carried out for the SKA Signal and Data Transport (SaDT) consortium as part of the SKA project. The SKA project is an international effort to build the world's largest radio telescope, led by the SKA Organization with the support of 10 member countries. Fourteen institutions from eight countries are involved in the SaDT consortium, led by the University of Manchester.

This work was supported by the Program of International S&T Cooperation under Grant No. 2016YFE0100200

References

1. B. Alachkar, P. Boven, and A. Wilkinson, "SKA1 Level 1 synchronisation and timing requirements analysis and verification," Available: https://xorg.manchester.ac.uk/sites/ska-sadt-dms/ (2017).
2. B. Wang, X. Zhu, C. Gao, Y. Bai, J. W. Dong, and L. J. Wang, Sci. Rep. **5**, 13851 (2015).
3. M. Fujieda, M. Kumagai, and S. Nagano, IEEE Trans. Ultrason. Ferroelectr. Freq. Control. **57**, 168 (2010).
4. V. Smotlacha and A. Kuna, in *Proceedings of European Frequency and Time Forum* (2012), p. 375.
5. O. Lopez, A. Haboucha, F. Kéfélian, H. Jiang, B. Chanteau, V. Roncin, C. Chardonnet, A. Amy-Klein, and G. Santarelli, Opt. Express **18**, 16849 (2010).
6. B. Wang, C. Gao, W. L. Chen, J. Miao, X. Zhu, Y. Bai, J. W. Zhang, Y. Y. Feng, T. C. Li, and L. J. Wang, Sci. Rep. **2**, 556 (2012).
7. K. Predehl, G. Grosche, S. Raupach, S. Droste, O. Terra, J. Alnis, T. Legero, T. Hänsch, T. Udem, R. Holzwarth, and H. Schnatz, Science **336**, 441 (2012).
8. S. Droste, F. Ozimek, T. Udem, K. Predehl, T. W. Hänsch, H. Schnatz, G. Grosche, and R. Holzwarth, Phys. Rev. Lett. **111**, 110801 (2013).
9. S. W. Schediwy, D. Gozzard, K. G. Baldwin, B. J. Orr, R. Bruce Warrington, G. Aben, and A. N. Luiten, Opt. Lett. **38**, 2893 (2013).
10. F. F. Yin, A. X. Zhang, Y. T. Dai, T. P. Ren, K. Xu, J. Q. Li, J. T. Lin, and G. S. Tang, Opt. Express **22**, 878 (2014).
11. B. Ning, S.Y. Zhang, D. Hou, J.T. Wu, Z.B. Li, and J.Y. Zhao, Sci. Rep. **4**, 5109 (2014).
12. C. E. Calosso, E. Bertacco, D. Calonico, C. Clivati, G. A. Costanzo, M. Frittelli, F. Levi, A. Mura, and A. Godone, Opt. Lett. **39**, 1177 (2014).
13. Ł. Śliwczyński and P. Krehlik, IEEE Trans. Ultrason. Ferroelectr. Freq. Control **62**, 412 (2015).
14. S. M. F. Raupach, A. Koczwara, and G. Grosche, Phys. Rev. A **92**, 41 (2015).
15. Y. Dong, Z. Liu, X. Wang, N. Deng, W. Xie, and W. Hu, Chin. Opt. Lett. **14**, 120006 (2016).
16. Q. Liu, S. Han, J. Wang, Z. Feng, W. Chen, N. Cheng, Y. Gui, H. Cai, and S. Han, Chin. Opt. Lett. **33**, 070602 (2016).
17. X. Yuan and B. Wang, Chin. Opt. Lett. **15**, 101202 (2017).
18. L. G. Cohen and J. W. Fleming, Bell Syst. Tech. J. **58**, 945 (1979).
19. A. H. Hartog, A. J. Conduit, and D. N. Payne, Opt. Quantum Electron. **11**, 265 (1979).
20. T. Musha, J. Kamimura, and M. Nakazawa, Appl. Opt. **21**, 694 (1982).
21. P. L. Heinzmann and R. U. Hofstetter, Proc. SPIE **854**, 71 (1985).
22. J. J. Carr, S. L. Saikkonen, and D. H. Williams, Fiber Integr. Opt. **9**, 393 (1990).
23. K. P. Zhong, N. Jia, T. J. Li, M. G. Wang, J. F. Chi, and J. Sun, Proc. SPIE **7847**, 78472N (2010).
24. T. J. Pinkert, O. Böll, L. Willmann, G. S. M. Jansen, E. A. Dijck, B. G. H. M. Groeneveld, R. Smets, F. C. Bosveld, W. Ubachs, K. Jungmann, K. S. E. Eikema, and J. C. J. Koelemeij, Appl. Opt. **54**, 728 (2015).
25. E. A. Elias, R. Cichota, H. H. Torriani, and Q. de Jong van Lier, Soil Sci. Soc. Am. J. **68**, 784 (2004).
26. Weather record from "Weather Underground," Available: https://www.wunderground.com/personal-weather-station/dashboard?ID=INORTHER41 (2017).
27. N. R. Newbury, P. A. Williams, and W. C. Swann, Opt. Lett. **32**, 3056 (2007).
28. M. Bousonville and J. Rausch, in *Proceedings of DIPAC09* (2009), p. 248.